JCTC Journal of Chemical Theory and Computation

Article

pubs.acs.org/JCTC

Strong Spin−Orbit Coupling Facilitates C−H Activation in the Reactions of Os^+ with CH_3F: Theoretical Investigations

Joonghan Kim,[‡,∥] Kiryong Hong,[†,∥] Hyun Kook Kim,[†] Yoon Sup Lee,*[,§] and Tae Kyu Kim*[,†]

[†]Department of Chemistry and Chemistry Institute of Functional Materials, Pusan National University, Busan 609-735, Republic of Korea

[‡]Department of Chemistry, The Catholic University of Korea, Bucheon, 420-743, Republic of Korea

[§]Department of Chemistry, KAIST, Daejeon 305-701, Republic of Korea

Supporting Information

ABSTRACT: The relativistic effects are essential for a complete understanding of the reactions involving heavy transition metal cations with hydrocarbons. Despite this, spin−orbit coupling (SOC) *along* the reaction pathway is rarely considered. In this work, we demonstrate an unusual SOC on the chemical reactivity of a reaction of Os^+ with methyl fluoride (CH_3F) using density functional theory (DFT), high-level ab initio, and spin−orbit multiconfigurational ab initio methods. With the inclusion of the SO effect in the relevant potential energy surfaces (PESs), C−H bond activation by an Os^+ cation occurs readily *via* almost barrierless (about 2 kcal/mol) PESs of the SO coupled ground state. In contrast, a substantial reaction barrier was observed for C−F bond activation. The calculated results are in line with recent systematic experimental findings for reactions of transition metal cations with CH_3F. These results show that the SO effect can facilitate specific bond activation in chemical reactions associated with catalytic transition metal cations.

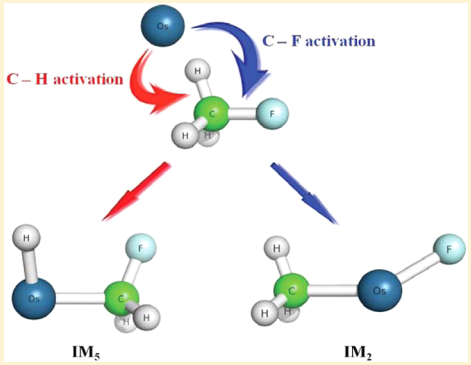

I. INTRODUCTION

Chemical reactions of small organic molecules with transition metal ions have prompted extensive studies aiming at unraveling the catalytic activities of transition metals. Systematic investigations of a series of transition metal ions with a range of organic molecules have provided a valuable understanding of specific bond activation, such as C−H activation. For this purpose, numerous studies have examined the reactions of transition metal ions (or complexes) with hydrocarbons.[1] Methane, which is the simplest hydrocarbon, has served as a model substrate for C−H activation by transition metal ions. In particular, third-row transition metal ions, such as Ta^+, W^+, Os^+, Ir^+, and Pt^+, are more efficient in reacting with methane *via* dehydrogenation than their first- and second-row analogs.[2] Specifically, spin−orbit coupling (SOC), which is intrinsically large for third-row transition metals, can facilitate a spin-state change during a reaction involving transition metal ions. Many theoretical studies have been performed to examine the reactivity of third-row transition metal ions, but generally, only scalar relativistic effects on the reaction pathways have been considered.[1d,3] On the other hand, the inclusion of the expected large SOC may be essential for the quantitative descriptions of reactivity associated with third-row transition metal ions. To examine this factor, the reaction potential energy surfaces (PESs) including SOC are required. Therefore, the SO-coupled reaction PESs should be examined. In a few studies, SOC was considered on the structures of intermediates and transition states optimized at the scalar relativistic level.[4] However, when SOC is large as in the case of 5d transition metal ions, this consideration might provide limited information for a realistic reaction pathway. The location of transition states and the activation barriers on the reaction PESs, including SOC, can significantly differ from those on the reaction PESs without SOC. Therefore, a consideration of SOC *along* the reaction PESs is essential for obtaining reliable and quantitative information on the reaction pathways of third-row transition metal ions with organic molecules. For this purpose, systematic DFT and SO multiconfigurational ab initio calculations were performed to elucidate the SO effect on the specific bond activation reactivity of Os^+-induced C−H and C−F activation processes of methyl fluoride (CH_3F), as shown in Figure 1.

CH_3F serves as a model to examine the competition between the C−H and C−F activation. The reactivity of CH_3F with various transition metal ions has been well established experimentally.[5] Bohme and co-workers examined the reactions of CH_3F with a number of atomic cations systematically using an inductively coupled plasma/selected-ion flow tube tandem mass spectrometer.[3a,5] Product distributions and rate constants were measured. Primary reaction channels, which are correlated with periodicities of atomic cations, were observed in F-atom transfer, CH_3F addition (clustering), HF elimination, and dehydrogenation. The dehydrogenation channel dominates the

Received: November 28, 2012
Published: January 17, 2013

   dx.doi.org/10.1021/ct301041u | J. Chem. Theory Comput. 2013, 9, 1087−1092

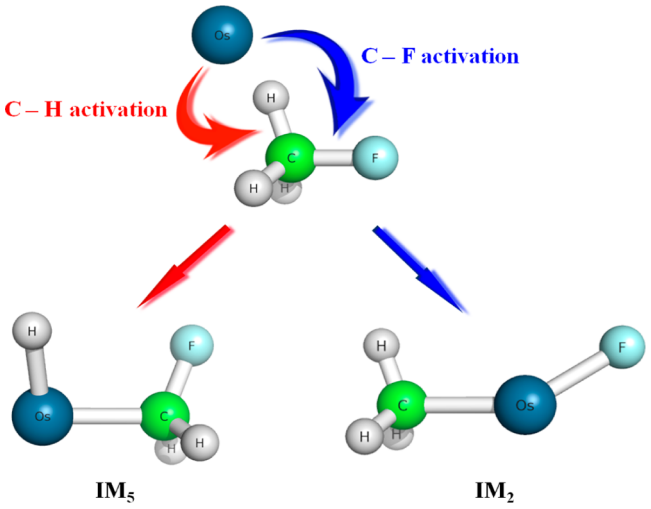

Figure 1. Schematic diagram of the C−H and C−F activation by an Os^+ ion and their related reaction intermediates (IM_5 and IM_2).

reactions of W^+, Os^+, Ir^+, and Pt^+. In the case of Os^+, the dehydrogenation pathway is the primary reaction with an exclusive product ratio of 0.98 and a rate constant of 1.8×10^{-10} cm^3 $molecule^{-1}$ s^{-1} at 295 ± 2 K. Therefore, previous studies indicate that the reaction of CH_3F with Os^+ provides an opportunity for competition between the C−H and C−F activation to the dehydrogenation pathway. In the present study, the reaction energy profiles for the reaction of Os^+ with CH_3F were calculated, and the SO effect along these reaction pathways was examined.

II. COMPUTATIONAL DETAILS

The reaction PESs of the doublet, quartet, and sextet spin states were calculated using the DFT method. All geometries of the reaction species (reactants, intermediates, products, and transition states) were fully optimized using the PBE0 hybrid functional.[6] According to recent investigations, the PBE0 functional shows good performance for molecular structures involving 5d transition metals.[7] Therefore, PBE0 was selected to optimize the molecular structures. The relativistic effective core potential (RECP) was used to treat the scalar relativistic effect for Os. The energy-consistent pseudopotentials with the correlation consistent basis set, aug-cc-pVTZ-pp reported by Figgen et al.[8] and aug-cc-pVTZ all-electron basis sets[9] were used for Os and the other atoms (C, H, and F), respectively. All transition states were identified by one imaginary frequency and confirmed using the intrinsic reaction coordinate (IRC) method. The single-point energy calculations were also carried out using the CCSD(T) method[10] to obtain more accurate energies for all relevant species. In the CCSD(T) single-point calculations, the optimized geometries of the reaction species using PBE0 were employed (CCSD(T)/aug-cc-pVTZ//PBE0/aug-cc-pVTZ). The zero point energy (ZPE) calculated by PBE0 was used for the correction. Natural population analysis (NPA)[11] was also used to characterize the atomic charges and electronic structures. The Gaussian 03 program[12] was used for all DFT and CCSD(T) calculations. The Gaussian 09 program[13] was used for geometry optimizations and IRC calculations of the transition state between intermediates 5 and 6 of the doublet state (denoted as $^2TS_{56}$). In this case, the reaction PESs in the IRC calculations calculated by Gaussian 03 show discontinuity. $^6Os^+$ (the superscript denotes the spin multiplicity) with CH_3F was used as the reference energy of all reaction PESs. Therefore, all energy values are relative to the reference energy.

The complete active space self-consistent field (CASSCF) method[14] was used to calculate some important reaction PESs. The active orbitals could not be maintained in some state-specific (SS) CASSCF calculations due to the participation of excited states. In such cases, the state-average (SA) CASSCF was used. The "SA*n*" means that *n* states were averaged in the SA-CASSCF calculation. The segmented all-electron relativistically contracted (SARC) TZVP ([17s11p8d3f]) basis set was used for the Os atom.[15] For other atoms, the basis set size was reduced by excluding the diffuse function, cc-pVTZ, due to the extensive computation time. The Douglas−Kroll−Hess second-order method (DKH2) was used to consider the scalar relativistic effect.[16] Therefore, the SARC-DKH2 TZVP basis set was used for Os and cc-pVTZ, whose contraction coefficient was reoptimized to be optimal for the DKH2 calculations of other atoms. Spin−orbit multiconfigurational quasi-degenerate perturbation theory (SO-MCQDPT) was used to consider the dynamic electron correlation and SOC.[17] All electrons of the

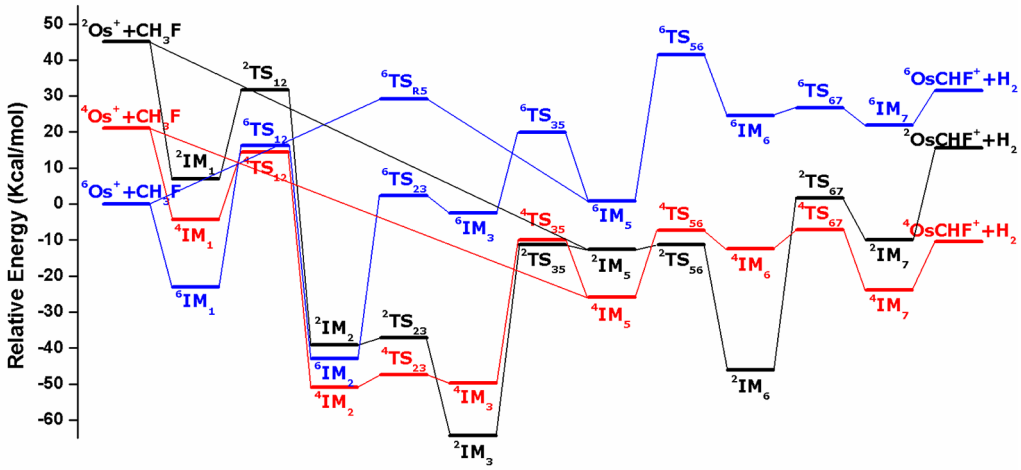

Figure 2. Reaction PESs of the H_2 elimination pathway calculated by CCSD(T)/aug-cc-pVTZ//PBE0/aug-cc-pVTZ. The related optimized molecular structures and relative energies are shown in Figure S1 in the Supporting Information.

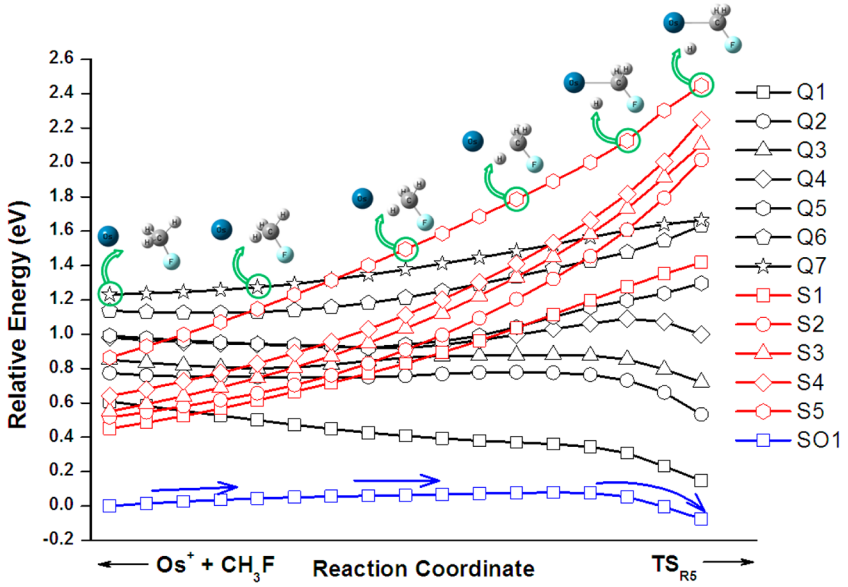

Figure 3. Reaction PESs (regarding C−H activation) according to the reverse IRC pathway from $^6TS_{R5}$ to $Os^+ + CH_3F$ (reactant) using the SO-MCQDPT method. The black, red, and blue lines show the quartet (Q), sextet (S), and ground SO coupled states (SO1), respectively.

Os^+−CH_3F complex were correlated in the MCQDPT2 calculations. The full Breit−Pauli Hamiltonian was used for the spin-dependent Hamiltonian. Seven quartet and five sextet PESs converge into two states, ^4F and ^6D, respectively, in the dissociation limit ($Os^+ + CH_3F$). The energy difference between the ^4F and ^6D states calculated by MCQDPT2 at the 10 Å C−Os^+ separation was 24.2 kcal/mol (21.1 kcal/mol at the CCSD(T) level), suggesting that the selection of the active orbitals and all-electron basis sets is reasonable. In addition, SO splitting among the SO coupled states of the Os^+ ion by SO-MCQDPT were 0.0 ($^6D_{9/2}$), 3217 ($^6D_{7/2}$), 4382 ($^6D_{5/2}$), 5502 ($^6D_{3/2}$), and 6153 cm^{-1} ($^6D_{1/2}$), which are close to the experimental results (0.0, 3593.15, 3928.94, 5592.05, and 6636.57 cm^{-1}).[18] These findings indicate that the SO-MCQDPT method can reasonably treat the SOC and dynamic correlation effects simultaneously. All CASSCF and SO-MCQDPT calculations were performed using the GAMESS code.[19] In addition, the validity of PBE0 and CCSD(T) for calculation of the activation barrier is discussed in the Supporting Information.

III. RESULTS AND DISCUSSION

The dehydrogenation pathway on the reaction of Os^+ with CH_3F can be initiated *via* either C−F or C−H activation. Reaction potential energy profiles in all spin states for the dehydrogenation pathway and relevant optimized molecular structures for reactants, intermediates (IM), and transition states (TS) are shown in Figures 2 and S1, respectively. Initially, the Os^+ ion attacks the electron-rich F atom of CH_3F, forming a stable association complex (IM_1) in all spin states. The natural population analysis (NPA) charge of the F atom of CH_3F is −0.376. Once an association complex is formed, the Os^+ ion can be inserted into the C−F bond *via* a transition state, TS_{12}. The Os^+ ion readily activates the C−F bond of CH_3F (C−F activation) forming IM_2. The Os atom lies between C and F atoms on the IM_2 structures in all spin states (see $^2IM_2$, $^4IM_2$, and $^6IM_2$ in Figure S1). A scissor vibration of C−Os^+−H in IM_2 can allow one of the H atoms of the methyl group to migrate to the Os atom *via* TS_{23}, forming IM_3. As shown in Figure 2, only the pathway in the sextet spin-state presents a relatively high reaction barrier between $^6IM_2$ and $^6TS_{23}$ (PBE0: 44.5 and CCSD(T): 45.3 kcal/mol), indicating that the proceeding reaction on the sextet PES is less favorable than the other spin states. The F atom then migrates to a C atom *via* TS_{35}, which involves a bridged structure in all spin-states. Once the F atom is attached to the C atom, IM_5 forms. As shown in Figure 1, IM_5 is closely related to C−H activation in the dehydrogenation reaction, and this feature will be discussed later. After IM_5, IM_6 is formed as a result of H atom migration from the CH_2F moiety *via* TS_{56}. An internal rotation of H−Os^+−H gives rise to the formation of IM_7, which is a direct precursor of the products in the dehydrogenation channel ($OsCHF^+ + H_2$). Finally, H_2 can dissociate from IM_7. In the dehydrogenation pathway by C−F activation, the highest reaction barriers at the CCSD(T) scalar relativistic level were 53.0 (between $^2IM_3$ and $^2TS_{35}$), 39.8 (between $^4IM_3$ and $^4TS_{35}$), and 45.3 kcal/mol ($^6IM_2$ and $^6TS_{23}$) on the doublet, quartet, and sextet spin states, respectively. These relatively high reaction barriers suggest that the dehydrogenation reaction pathway by C−F activation is unlikely. This finding is in contrast to the experimental observations that the dehydrogenation pathway is the dominant process.[5] On the other hand, the highest reaction barriers in all spin-states are located just before IM_5, which is the most likely intermediate in the C−H activated dehydrogenation pathway. Therefore, another possibility, a reaction starting from C−H activation, should also be examined.

The C−H activation in the dehydrogenation pathway also starts from the reactants, Os^+ and CH_3F. Subsequently, an Os^+ ion can be inserted into the C−H bond, forming IM_5. Despite the considerable efforts aimed at finding the transition state between the reactants and IM_5, only one transition state on the sextet state ($^6TS_{R5}$) has been identified (see Figures 2 and S1). This is similar to the reaction between Os^+ and CH_4, in which only one transition state on the sextet state is located during C−H activation by Os^+.[1d] However, C−H activation by the Os^+ ion on the sextet PES cannot readily occur due to the relatively high reaction barrier between the reactants and $^6TS_{R5}$ (29.2

dx.doi.org/10.1021/ct301041u | J. Chem. Theory Comput. 2013, 9, 1087−1092

kcal/mol at the CCSD(T) level). In addition, because the energy difference between the sextet (^{6}D) and quartet (^{4}F) of the Os^+ ion is 21.1 kcal/mol (see Figure 2),[1d,3b] only the sextet state of the Os^+ ion can be populated initially. Moreover, after C−H activation, $^6IM_5$ lies at a higher energy than $^4IM_5$ and $^2IM_5$, meaning different energy ordering of spin states. This suggests that intersystem crossing (ISC) should exist between the reactants ($Os^+ + CH_3F$) and IM_5 on the C−H activated dehydrogenation pathway. Therefore, it might be directly related to the enhanced *reactivity via specific bond activation* in the dehydrogenation pathway. A previous DFT study on the reaction of Os^+ with CH_4 suggested that ISC exists and is caused by SOC, but the SO effect on ISC has not been identified: only doublet, quartet, and sextet PESs have been calculated and considered separately.[1d] To resolve the ISC and SO effects, which are crucial for specific bond activation, the reaction PESs along the reverse IRC[20] path of $^6TS_{R5}$ (from $^6TS_{R5}$ to the reactants, $Os^+ + CH_3F$) was examined using SO-MCQDPT (Figure 3). This approach was suggested by Yoshizawa et al.[1c,21] The active orbitals for the CASSCF calculations are shown in Figure S2. The state-average (SA) CASSCF was used because the PESs are correlated asymptotically into the ^{6}D (five states) and ^{4}F (seven states) states of the Os^+ ion at the dissociation limit of Os^+ and CH_3F. The molecular structures on the selected IRC points in Figure 3 clearly show how the Os^+ ion activates the C−H bond in CH_3F. ISC between the lowest sextet (S1) and quartet (Q1) states occurs at the initial stage of C−H activation. The SO effect along the reaction pathway, IRC points, was considered. A total of 58 SO coupled states were generated, but only the SO ground state is shown for clarity (blue line in Figure 3). The calculated ground SO state energy indicates that a consideration of the SO effect reduces the reaction barrier substantially. Therefore, SOC should be included in the reaction of Os^+ and CH_3F. PESs without SOC, such as quartet and sextet PESs, cannot describe the actual PESs of Os^+ with CH_3F. When the ground state of Os^+ ($^6D_{9/2}$) approaches CH_3F, C−H activation should proceed *via* a SO coupled ground state. Interestingly, this process is almost a *barrierless process* whose barrier height is approximately 2 kcal/mol. This barrier height was estimated from the difference between the energy at the summit of the SO coupled ground state PES and that of Os^+ with CH_3F at a 10 Å separation. This result implies that a strong SO effect greatly facilitates C−H activation in the dehydrogenation process and enhances the reactivity *via* specific bond activation. A recent study[4b] reported that the SO effect of the transition metal complexes (involving ligated Ir and Pt complexes) increases the C−H activation barrier. This result appears to be in contrast to the present results. However, the magnitude of SOC in the transition metal complex is much smaller than that of the transition metal ion, because the ligand field of the transition metal complex quenches SOC. For the transition metal complexes with closed shell configurations, the SOC becomes quite insignificant, being almost less than 1 kcal/mol.[4b] Therefore, the result of the previous study does not conflict with those obtained in the present study.

The minimum energy crossing point (MECP, ISC) between the S1 and Q1 states was optimized (see Figure S3) using state-specific CAS(11,10). On the basis of these results, ISC occurs during C−H activation (Os^+ ion is inserted into one of the C−H bonds in CH_3F), and the reaction finally reaches IM_5 after passing through ISC.

The SO effect reduces the reaction barrier of C−H activation on the dehydrogenation pathway. ISC also can occur in C−F activation considering the energy reversal between the quartet and sextet states from IM_1 to IM_2. Therefore, the same approach using the SO-MCQDPT method was applied to the reaction PESs from IM_1 to IM_2 according to the IRC pathways of the sextet state. SA9-CAS(13,10) was used as the reference wave function for the SO-MCQDPT calculations. Figure S4 shows the active orbitals. Reaction PESs along the IRC coordinates on the C−F activated dehydrogenation pathway using the SO-MCQDPT method are depicted in Figure 4.

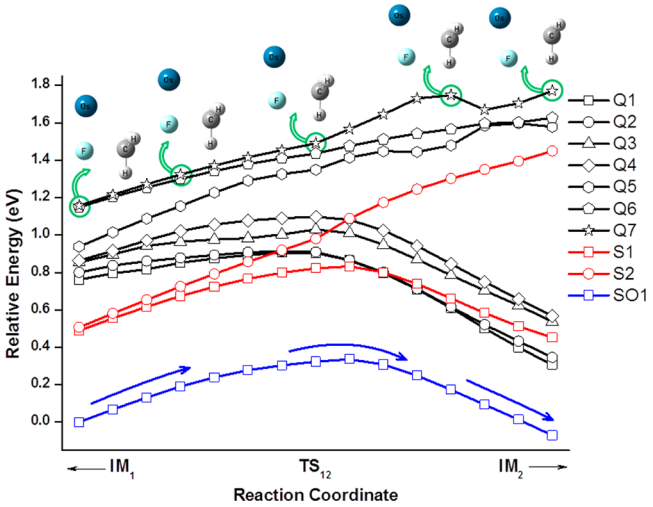

Figure 4. Reaction PESs (regarding C−F activation) according to IRC pathway from $^6TS_{12}$ to both $^6IM_1$ and $^6IM_2$ using the SO-MCQDPT method. The black, red, and blue lines show the quartet (Q), sextet (S), and ground SO coupled states (SO1), respectively.

Unlike C−H activation, a substantial reaction barrier was clearly observed on the PES of the SO coupled ground state. The estimated reaction barrier height using SO-MCQDPT, which was calculated from the difference between the energy of the top point on the SO coupled ground state and that of the right end point on the IRC reverse coordinates, was approximately 21.7 kcal/mol. The actual barrier height should be more than 21.7 kcal/mol. C−F activation is unlikely to occur compared to C−H activation in the dehydrogenation pathway due to the large activation barrier.

The HF elimination pathway (see Figure S5) was also investigated to explain the experimental findings indicating the dominant occurrence of the dehydrogenation pathway because this channel can also be initiated from either C−H or C−F activation. In the C−F activated HF elimination channel, the energy profiles up to IM_3 are the same as those in the dehydrogenation pathway. After IM_2, there are two alternative reaction pathways: one *via* TS_{24} and the other *via* TS_{23}. As shown in Figure S6, the F atom connected to the Os atom withdraws one of the H atoms from the methyl group, forming a four-membered ring structure (TS_{24}) in all spin states. This process is unlikely to occur due to the high reaction barrier. In another plausible pathway, the F atom in IM_3 attracts an H atom that is already attached to the Os atom *via* TS_{34}, producing IM_4 in all spin states. The distance between the H and F atoms is close to the H−F bond distance of the HF molecule. Finally, the products ($OsCH_2^+$ and HF) are formed.

The HF elimination reaction can also start from C−H activation, as in the dehydrogenation pathway, with the initial reactants reaching IM_5 *via* a barrierless SO coupled state. The F atom migrates to the Os atom *via* TS_{35}, which shows three-membered ring structures (see Figure S1), and IM_3 then forms in all spin states. Finally, the reaction proceeds to IM_4 *via* TS_{34}, which is precisely the same as C−F activation, as explained above. IM_4 is the final intermediate of the C−H or C−F-activated HF elimination pathway. In the HF elimination reactions, the reaction barrier can be estimated from the relative energies calculated at the CCSD(T) scalar relativistic level. Although the inclusion of SOC along the reaction pathway gives more accurate results, the trend of the magnitude of the reaction barrier can be estimated on the scalar relativistic level (a detailed study of SO-coupled PESs is in progress). In the HF elimination pathway, the barrier between $^4IM_3$ and $^4TS_{34}$ (37.3 kcal/mol at the scalar relativistic level) is the highest, whereas that of the dehydrogenation reaction between $^4IM_5$ and $^4TS_{56}$ is 18.6 kcal/mol, which is only half that of the HF elimination pathway. Although the real reaction barriers may be smaller than those estimated in the scalar relativistic level, the barrier height of HF elimination should be much higher than that of the dehydrogenation pathway, even after including SOC. These findings suggest that the dehydrogenation pathway is a more feasible route, which is in good agreement with the recent experimental findings.[5] The direct comparison between calculation results and literature values[5] is not attempted here since only the rate constant and the product distribution for the dehydrogen channel were reported. In addition, the C−H/C−F bond activation ratio for the dehydrogenation channel has not been experimentally investigated.

The calculation results imply two major findings: (1) The dehydrogenation pathway is a more efficient route than the HF elimination channel. (2) During the C−H and C−F activated dehydrogenation pathways, the strong SOC of the Os^+ ion induces C−H activation *via* an almost barrierless SO coupled state. These findings show that the *specific bond reactivity* is associated with the *strong SOC*.[22] Zhao et al. examined the reactions of 5d transition metal ions (from W^+ to Pt^+) with CH_3F along with their counterparts of 4d (from Mo^+ to Pd^+, except Tc^+) and 3d metal ions (from Cr^+ to Co^+).[5] All the reactions with 5d metal ions (except Re^+) revealed the dehydrogenation channel to be the dominant pathway. In contrast, all those 4d and 3d metal ions had no reactivity; the major product is *clustering* with CH_3F. These experimental results strongly correlate with the SOC strength of 5d transition metal ions. A strong SOC of 5d metal ions induces the C−H activation of CH_3F. On the other hand, a relatively weak SOC of 4d and 3d transition metal ions does not invoke a chemical event (C−H activation). In the case of Re^+, the SOC of Re^+ is too weak to initiate C−H activation due to the ground electronic configuration of $5d^56s$ (^7S state), and clustering with CH_3F is the primary channel, as in the 4d and 3d metal ions cases.

IV. CONCLUSIONS

Calculations with SO multiconfigurational ab initio and DFT methods were performed to examine the reaction of Os^+ with CH_3F. SOC along the reaction pathways was considered. The calculated results showed that a strong SOC enhances the activation of a specific bond, C−H activation. In addition, the calculations can explain the recent experimental findings; the dominance of the dehydrogenation pathway on the reactions of 5d metal ions with CH_3F. This is the first report showing that the specific bond reactivity is affected by strong SOC.

■ ASSOCIATED CONTENT

Ⓢ Supporting Information

Optimized molecular structures of all reaction species, active orbitals for CAS(11,10) and CAS(13,10) calculations, MECP between S1 and Q1 and its optimized molecular structure, and reaction PESs of HF elimination. This material is available free of charge via the Internet at http://pubs.acs.org.

■ AUTHOR INFORMATION

Corresponding Author

*E-mail: tkkim@pusan.ac.kr, yslee@kaist.edu.

Author Contributions

‖These authors contributed equally.

Notes

The authors declare no competing financial interest.

■ ACKNOWLEDGMENTS

This work was supported by National Research Foundation of Korea (NRF) grants funded by the Korean government (MEST) (No. 2007-0056330, 2007-0056341, 2009-0068446, and 2010-0006570). T.K.K also greatly acknowledges support by Global Research Laboratory (No. 2011-00131), by Leading Foreign Research Institute Recruitment Program (No. 2010-00471), and by Max Plank POSTECH/KOREA Research Initiative Program (No. 2011-0031558) through the NRF funded by MEST.

■ REFERENCES

(1) (a) van Koppen, P. A. M.; Brodbelt-Lustig, J.; Bowers, M. T.; Dearden, D. V.; Beauchamp, J. L.; Fisher, E. R.; Armentrout, P. B. Transition Metal Ion Mediated C−H and C−C Bond Activation of Alkanes: Dynamical Coupling Between Entrance and Exit Channel Transition States. *J. Am. Chem. Soc.* **1991**, *113*, 2359−2369. (b) Holthausen, M. C.; Fiedler, A.; Schwarz, H.; Koch, W. How Does Fe^+ Activate C−C and C−H Bonds in Ethane? A Theoretical Investigation Using Density Functional Theory. *J. Phys. Chem.* **1996**, *100*, 6236−6242. (c) Shiota, Y.; Yoshizawa, K. A Spin-Orbit Coupling Study on the Spin Inversion Processes in the Direct Methane-to-Methanol Conversion by FeO^+. *J. Chem. Phys.* **2003**, *118*, 5872−5879. (d) Zhang, G.; Li, S.; Jiang, Y. Dehydrogenation of Methane by Gas-Phase Os^+: A Density Functional Study. *Organometallics* **2003**, *22*, 3820−3830. (e) Schröder, D.; Schwarz, H. Gas-Phase Activation of Methane by Ligated Transition-Metal Cations. *Proc. Natl. Acad. Sci. U. S. A.* **2008**, *105*, 18114−18119. (f) Lv, L.; Wang, Y.; Wang, Q.; Liu, H. Why is Pt_4^+ the Least Efficient Cationic Cluster in Activating the C−H Bond in Methane? Two-State Reaction Computational Investigation. *J. Phys. Chem. C* **2010**, *114*, 17610−17620. (g) Balcells, D.; Clot, E.; Eisenstein, O. C−H Bond Activation in Transition Metal Species from a Computational Perspective. *Chem. Rev.* **2010**, *110*, 749−823. (h) Roithová, J.; Schröder, D. Selective Activation of Alkanes by Gas-Phase Metal Ions. *Chem. Rev.* **2010**, *110*, 1170−1211.

(2) (a) Irikura, K. K.; Beauchamp, J. L. Methane Oligomerization in the Gas Phase by Third-Row Transition-Metal Ions. *J. Am. Chem. Soc.* **1991**, *113*, 2769−2770. (b) Irikura, K. K.; Beauchamp, J. L. Electronic Structure Considerations for Methane Activation by Third-Row Transition-Metal Ions. *J. Phys. Chem.* **1991**, *95*, 8344−8351. (c) Buckner, S. W.; MacMahon, T. J.; Byrd, G. D.; Freiser, B. S. C−H Bond Activation and Ligand-Coupling Mechanisms. *Inorg. Chem.* **1989**, *28*, 3511−3518. (d) Li, F.-X.; Zhang, X.-G.; Armentrout, P. B. The Most Reactive Third-Row Transition Metal: Guided Ion Beam and Theoretical Studies of the Activation of Methane by Ir^+. *Int. J. Mass Spectrom.* **2006**, *255−256*, 279−300.

(3) (a) Zhao, X.; Hopkinson, A. C.; Bohme, D. K. Competitive Activation of C−H and C−X Bonds in Reactions of Pt^+ with CH_3X (X=F, Cl): Experiment and Theory. *ChemPhysChem.* **2008**, *9*, 873−881. (b) Li, T. H.; Wang, C. M.; Yu, S. W.; Liu, X. Y.; Li, X. H.; Xie, X. G. A Theoretical Study on the Gas Phase Reaction of Au^+ with CH_3F. *Chem. Phys. Lett.* **2008**, *463*, 334−339.

(4) (a) Danovich, D.; Shaik, S. Spin-Orbit Coupling in the Oxidative Activation of H−H by FeO^+. Selection Rules and Reactivity Effects. *J. Am. Chem. Soc.* **1997**, *119*, 1773−1786. (b) Chen, K.; Zhang, G.; Chen, H.; Yao, J.; Danovich, D.; Shaik, S. Spin-Orbit Coupling and Outer-Core Correlation Effects in Ir- and Pt-Catalyzed C−H Activation. *J. Chem. Theory Comput.* **2012**, *8*, 1641−1645.

(5) Zhao, X.; Koyanagi, G. K.; Bohme, D. K. Reactions of Methyl Fluoride with Atomic Transition-Metal and Main-Group Cations: Gas-Phase Room-Temperature Kinetics and Periodicities in Reactivity. *J. Phys. Chem. A* **2006**, *110*, 10607−10618.

(6) Adamo, C.; Barone, V. Toward Reliable Density Functional Methods without Adjustable Parameters: The PBE0Model. *J. Chem. Phys.* **1999**, *110*, 6158−6170.

(7) (a) Bühl, M.; Reimann, C.; Pantazis, D. A.; Bredow, T.; Neese, F. Geometries of Third-Row Transition-Metal Complexes from Density-Functional Theory. *J. Chem. Theory Comput.* **2008**, *4*, 1449−1459. (b) Kim, J.; Ihee, H.; Lee, Y. S. Spin-Orbit Density Functional and Ab Initio Study of HgXn (X = F, Cl, Br, and I; n = 1, 2, and 4). *J. Chem. Phys.* **2010**, *133*, 144309.

(8) Figgen, D.; Peterson, K. A.; Dolg, M.; Stoll, H. Energy-Consistent Pseudopotentials and Correlation Consistent Basis Sets for the 5d Elements Hf−Pt. *J. Chem. Phys.* **2009**, *130*, 164108.

(9) (a) Dunning, T. H. Gaussian Basis Sets for Use in Correlated Molecular Calculations. I. The Atoms Boron through Neon and Hydrogen. *J. Chem. Phys.* **1989**, *90*, 1007−1023. (b) Kendall, R. A.; Dunning, T. H.; Harrison, R. J. Electron Affinities of the First-Row Atoms Revisited. Systematic Basis Sets and Wave Functions. *J. Chem. Phys.* **1992**, *96*, 6796−6806.

(10) Raghavachari, K.; Trucks, G. W.; Pople, J. A.; Head-Gordon, M. A Fifth-Order Perturbation Comparison of Electron Correlation Theories. *Chem. Phys. Lett.* **1989**, *157*, 479−483.

(11) Reed, A. E.; Weinstock, R. B.; Weinhold, F. Natural Population Analysis. *J. Chem. Phys.* **1985**, *83*, 735−746.

(12) Frisch, M. J.; Trucks, G. W.; Schlegel, H. B.; Scuseria, G. E.; Robb, M. A.; Cheeseman, J. R.; Montgomery, J. A., Jr.; Vreven, T.; Kudin, K. N.; Burant, J. C.; Millam, J. M.; Iyengar, S. S.; Tomasi, J.; Barone, V.; Mennucci, B.; Cossi, M.; Scalmani, G.; Rega, N.; Petersson, G. A.; Nakatsuji, H.; Hada, M.; Ehara, M.; Toyota, K.; Fukuda, R.; Hasegawa, J.; Ishida, M.; Nakajima, T.; Honda, Y.; Kitao, O.; Nakai, H.; Klene, M.; Li, X.; Knox, J. E.; Hratchian, H. P.; Cross, J. B.; Adamo, C.; Jaramillo, J.; Gomperts, R.; Stratmann, R. E.; Yazyev, O.; Austin, A. J.; Cammi, R.; Pomelli, C.; Ochterski, J. W.; Ayala, P. Y.; Morokuma, K.; Voth, G. A.; Salvador, P.; Dannenberg, J. J.; Zakrzewski, V. G.; Dapprich, S.; Daniels, A. D.; Strain, M. C.; Farkas, O.; Malick, D. K.; Rabuck, A. D.; Raghavachari, K.; Foresman, J. B.; Ortiz, J. V.; Cui, Q.; Baboul, A. G.; Clifford, S.; Cioslowski, J.; Stefanov, B. B.; Liu, G.; Liashenko, A.; Piskorz, P.; Komaromi, I.; Martin, R. L.; Fox, D. J.; Keith, T.; Al-Laham, M. A.; Peng, C. Y.; Nanayakkara, A.; Challacombe, M.; Gill, P. M. W.; Johnson, B.; Chen, W.; Wong, M. W.; Gonzalez, C.; Pople, J. A. *Gaussian 03*, Revision C.02; Gaussian, Inc.: Wallingford, CT, 2004.

(13) Frisch, M. J.; Trucks, G. W.; Schlegel, H. B.; Scuseria, G. E.; Robb, M. A.; Cheeseman, J. R.; Scalmani, G.; Barone, V.; Mennucci, B.; Petersson, G. A.; Nakatsuji, H.; Caricato, M.; Li, X.; Hratchian, H. P.; Izmaylov, A. F.; Bloino, J.; Zheng, G.; Sonnenberg, J. L.; Hada, M.; Ehara, M.; Toyota, K.; Fukuda, R.; Hasegawa, J.; Ishida, M.; Nakajima, T.; Honda, Y.; Kitao, O.; Nakai, H.; Vreven, T.; Montgomery, J. A., Jr.; Peralta, J. E.; Ogliaro, F.; Bearpark, M.; Heyd, J. J.; Brothers, E.; Kudin, K. N.; Staroverov, V. N.; Keith, T.; Kobayashi, R.; Normand, J.; Raghavachari, K.; Rendell, A.; Burant, J. C.; Iyengar, S. S.; Tomasi, J.; Cossi, M.; Rega, N.; Millam, J. M.; Klene, M.; Knox, J. E.; Cross, J. B.; Bakken, V.; Adamo, C.; Jaramillo, J.; Gomperts, R.; Stratmann, R. E.; Yazyev, O.; Austin, A. J.; Cammi, R.; Pomelli, C.; Ochterski, J. W.; Martin, R. L.; Morokuma, K.; Zakrzewski, V. G.; Voth, G. A.; Salvador, P.; Dannenberg, J. J.; Dapprich, S.; Daniels, A. D.; Farkas, O.; Foresman, J. B.; Ortiz, J. V.; Cioslowski, J.; Fox, D. J. *Gaussian 09*, revision B.01; Gaussian, Inc.: Wallingford, CT, 2010.

(14) Roos, B. O. *Advances in Chemical Physics: Ab Initio Methods in Quantum Chemistry II*; Lawley, K. P., Eds.; John Wiley and Sons: Chichester, England, 1987; pp 399−445.

(15) Pantazis, D. A.; Chen, X.-Y.; Landis, C. R.; Neese, F. All-Electron Scalar Relativistic Basis Sets for Third-Row Transition Metal Atoms. *J. Chem. Theory Comput.* **2008**, *4*, 908−919.

(16) (a) Hess, B. A. Relativistic Electronic-Structure Calculations Employing a Two-Component No-Pair Formalism with External-Field Projection Operators. *Phys. Rev. A* **1986**, *33*, 3742−3748. (b) Jansen, G.; Hess, B. A. Revision of the Douglas-Kroll Transformation. *Phys. Rev. A* **1989**, *39*, 6016−6017.

(17) Fedorov, D. G.; Finley, J. P. Spin-Orbit Multireference Multistate Perturbation Theory. *Phys. Rev. A* **2001**, *64*, 042502.

(18) Sansonetti, J. E.; Martin, W. C. Handbook of Basic Atomic Spectroscopic Data. *J. Phys. Chem. Ref. Data* **2005**, *34* (4), 1559−2259.

(19) Schmidt, M. W.; Baldridge, K. K.; Boatz, J. A.; Elbert, S. T.; Gordon, M. S.; Jensen, J. H.; Koseki, S.; Matsunaga, N.; Nguyen, K. A.; Su, S.; Windus, T. L.; Dupuis, M.; Montgomery, J. A., Jr. General Atomic and Molecular Electronic Structure System. *J. Comput. Chem.* **1993**, *14*, 1347−1363.

(20) (a) Gonzalez, C.; Schlegel, H. B. An Improved Algorithm for Reaction Path Following. *J. Chem. Phys.* **1989**, *90*, 2154−2161. (b) Gonzalez, C.; Schlegel, H. B. Reaction Path Following in Mass-Weighted Internal Coordinates. *J. Phys. Chem.* **1990**, *94*, 5523−5527.

(21) Yoshizawa, K.; Shiota, Y.; Yamabe, T. Intrinsic Reaction Coordinate Analysis of the Conversion of Methane to Methanol by an Iron-Oxo Species: A Study of Crossing Seams of Potential Energy Surfaces. *J. Chem. Phys.* **1999**, *111*, 538−545.

(22) (a) Johansson, E. M. J.; Odelius, M.; Plogmaker, S.; Gorgoi, M.; Svensson, S.; Siegbahn, H.; Rensmo, H. Spin-Orbit Coupling and Metal-Ligand Interactions in Fe(II), Ru(II), and Os(II) Complexes. *J. Phys. Chem. C* **2010**, *114*, 10314−10322. (b) Srnec, M.; Chalupský, J.; Fojta, M.; Zendlová, L.; Havran, L.; Hocek, M.; Kývala, M.; Rulíšek, L. Effect of Spin-Orbit Coupling on Reduction Potentials of Octahedral Ruthenium(II/III) and Osmium(II/III) Complexes. *J. Am. Chem. Soc.* **2008**, *130*, 10947−10954.